Determination of π-Meson Masses by Neutron Time of Flight*

JOHN B. CZIRR†
Lawrence Radiation Laboratory, University of California, Berkeley, California
(Received 26 November 1962)

Time-of-flight techniques were used to measure the velocities of the neutrons from the reactions, at rest, $\pi^-+p\rightarrow n+\pi^0$ and $\pi^-+p\rightarrow n+\gamma$. From these velocities the π^- mass and the π^--π^0 mass difference were obtained, with the results $m_{\pi^-}=139.69\pm0.41$ MeV/c^2 and $m_{\pi^-}-m_{\pi^0}=4.6056\pm0.0055$ MeV/c^2. The neutron velocity distribution about the mean velocity was measured and found to have an rms deviation of $(8.0\pm1.5)\times10^6$ cm/sec.

Negative π mesons from the 184-in. cyclotron were degraded by carbon and stopped in liquid hydrogen. The neutrons were detected in a plastic scintillator viewed by seven photomultiplier tubes. Time was measured for each event from the time of detection of a γ ray associated with that event. The γ-detector signal was delayed and photographed along with the neutron signal on an oscilloscope trace. Neutron times of flight were measured over distances of 17, 47, and 67 ft.

I. INTRODUCTION

A MEASUREMENT of the velocities of the neutrons arising from stopped negative pions in hydrogen affords a means of accurately determining the π^-mass and the $\pi^--\pi^0$ mass difference. In both the reactions at rest,

$$\pi^-+p\rightarrow\pi^0+n, \quad (1)$$

and

$$\pi^-+p\rightarrow\gamma+n, \quad (2)$$

the final-state neutrons have a unique velocity in the laboratory system which depends only on the rest masses involved. Previous experiments using this method have obtained the most accurate determinations of the $\pi^--\pi^0$ mass difference to date.[1] Other experiments determined the mass difference by measuring the Doppler shift in the energy,[2] or the angular correlation[3] of the γ rays from π^0 decay in order to determine the π^0 velocity. The present value for the mass difference[4] is 4.59 ± 0.05 MeV/c^2.

The most accurate determinations of the $\pi^\pm$ mass are of three types: (a) range-momentum,[5] (b) mesonic x rays,[6] and (c) γ energy from Reaction (2).[7] The combined result of these methods gives the value $m_{\pi^-}c^2=139.63\pm0.06$ MeV.[6]

This experiment was undertaken to greatly improve the $\pi^--\pi^0$ mass-difference determination and to obtain the π^- mass by the same technique. In addition, deviations about the mean velocity were observable and the velocity distribution of the slow neutrons from reaction (1) was determined.

II. EXPERIMENTAL TECHNIQUE

To reduce systematic errors in time-of-flight measurements it is desirable to measure the *difference* in flight time between two or more positions relative to the source. To reduce the fractional error in this case it becomes necessary to have the near distance small compared with the far distance.

The closest feasible distance is determined by considerations of background due to the incoming particles (not necessarily decreasing as $1/R^2$ from the target) and differences in path length due to finite target and detector size. At the Berkeley 184-in. cyclotron, the energy spread of the available beam of π^- mesons requires approx 12 in. of liquid hydrogen for an acceptable fraction of the particles to be stopped in hydrogen. For a neutron detector of approximately the same transverse dimension, a target-counter separation of 10 ft yields a flight-time variation of 2 nsec because of oblique flight paths. To eliminate sizeable corrections for this effect and because of shielding requirements, the distance from source to neutron detector was set at more than 10 ft. The maximum distance is determined primarily by the minimum useful signal-to-background ratio of the final data. The longest flight path used was 67 ft, at which distance the peak signal-to-background ratio was approximately unity. For larger distances, the signal-to-background ratio was less than unity because of a constant background level in the neutron counter.

Neutron time of flight was measured by displaying the start pulse [γ-detector output from $\pi^0-\gamma$ in re-

* Work done under the auspices of the U. S. Atomic Energy Commission.

† Present address: Physics Department, University of Washington, Seattle, Washington.

[1] M. Gettner, L. Holloway, D. Kraus, K. Lande, E. Leboy, and W. Selove, Phys. Rev. Letters **2**, 471 (1959); W. Selove and M. Gettner, Phys. Rev. **120**, 593 (1960); P. Hillman, W. C. Middlekoop, T. Yamagata, and E. Zavattini, Nuovo Cimento **14**, 887 (1959); R. Haddock, A. Abashian, K. Crowe, and J. Czirr, Phys. Rev. Letters **3**, 478 (1959).

[2] J. Kuehner, A. W. Merrison, and S. Tornabene, Proc. Phys. Soc. (London) (to be published).

[3] W. Chinowsky and J. Steinberger, Phys. Rev. **93**, 586 (1954); J. M. Cassels, D. P. Jones, P. G. Murphy, and P. L. O'Neill, Proc. Phys. Soc. (London) **74**, 92 (1959).

[4] W. H. Barkas and A. H. Rosenfeld, Lawrence Radiation Laboratory Report UCRL-8080-Rev. 1961 (unpublished). The error of ±0.05 MeV/c^2 is the best estimate of the error on the mass difference measured by Haddock *et al.*, Phys. Rev. Letters **3**, 478 (1959). The error of ±0.01 MeV/c^2 quoted by Barkas and Rosenfeld refers to a measurement by the same authors which was subject to larger systematic errors.

[5] W. H. Barkas, W. Birnbaum, and F. M. Smith, Phys. Rev. **101**, 778 (1956).

[6] E. R. Cohen, K. M. Crowe, and J. W. M. Dumond, *Fundamental Constants of Physics* (Interscience Publishers, Inc., New York, 1957).

[7] K. M. Crowe and R. H. Phillips, Phys. Rev. **96**, 470 (1954).

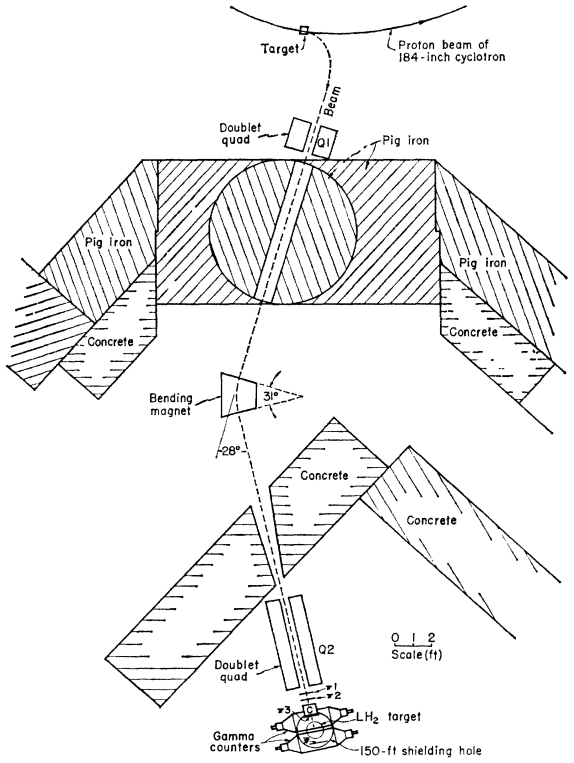

FIG. 1. Meson cave experimental setup.

action (1), or the 130-MeV γ in reaction (2)] and the neutron-detector signal on an oscilloscope and photographing the trace. The long time delay between these two events (of the order of microsceonds) was compensated for by delaying the γ signal through a low-attenuation delay line.

In order to minimize the spread in flight time of the neutrons, it was necessary to use a liquid-hydrogen target thin in the direction along the neutron flight path, and a thin neutron detector. Both of these dimensions were 1 in. in this experiment. The neutron detector consisted of a plastic-organic scintillator viewed by RCA 7046 photomultiplier tubes, thereby yielding time-of-arrival pulses with an intrinsic time spread of ± 4 nsec for the low-energy neutrons.

III. EXPERIMENTAL EQUIPMENT

To provide shielding for the neutron detector at all distances, a shielding hole 2 ft in diam and 150 ft deep was dug near the source of mesons from the cyclotron and lined with a vacuum-tight pipe. The neutron counter was moved vertically in this hole by means of a motor-driven cable drive. The hole was filled with He gas during the experiment, to reduce the neutron scattering in the long flight path.

A. Hydrogen Target and Meson Beam

A liquid-hydrogen target 1 ft in diam and 1 in. high was placed over the time-of-flight hole, in the beam of π^- mesons. This beam was deflected and focused by a bending magnet and two quadrupole magnets, and was measured to be 3.5 in. by 3.5 in. (full width at half-maximum) at the position of the target.

The bending magnet was provided with a pole tip having an 8-in.-high gap which was 24 in. transverse to the beam direction. A 31-deg wedge was chosen as the pole-tip shape in order to focus at the liquid-hydrogen target mesons of all momenta entering this magnet. The final quadrupole was placed as close as possible to the liquid-hydrogen target in order to minimize the magnification of the cyclotron meson target. The experimental setup is shown in Fig. 1.

The liquid-hydrogen container was constructed of 0.005-in. stainless steel. This container was enclosed in a stainless steel pressure dome 0.020 in. thick, and provided with vents such that the pressure was equal on the inside and outside of the liquid container. This in turn was contained in a vacuum tank with a 0.038-in. Al bottom dome, to permit the neutrons to escape downward. Carbon 33 g/cm^2 thick was placed in front of the target to degrade the beam energy and maximize the number of mesons stopping in the hydrogen.

B. Electronics and Counters

In order to minimize background, a coincidence was required among (a) the incoming beam monitor, (b) a γ detector placed above the target, and (c) two of the neutron-detector phototubes. The last requirement re-

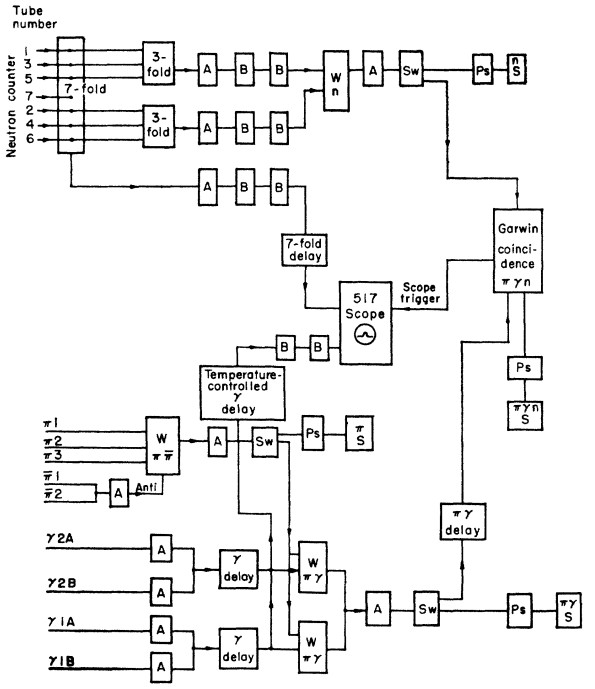

FIG. 2. Diagram of electronics. *A* and *B* refer to Hewlett-Packard 460 A and 460 B amplifiers, *W* to Wenzel coincidence circuits, *Sw* to Swift discriminators, *Ps* to Hewlett-Packard 520 prescalers, and *S* to scalers. (See reference 8 for details.)

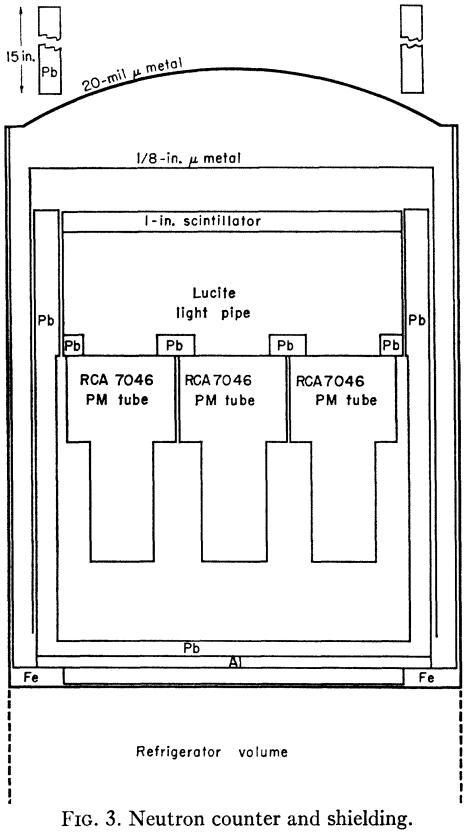

FIG. 3. Neutron counter and shielding.

duced the background due to phototube dark current to a negligible value. The above coincidence output was used to trigger an oscilloscope which used two traces of a four-trace oscilloscope tube attached to a Tektronix 517 A. The sum of all neutron-counter tubes was displayed on one trace and the sum of the γ-counter tubes was displayed on the other at a sweep speed of approx 20 nsec/cm. A diagram of the electronics is shown in Fig. 2.

The π monitor consisted of two $\frac{1}{4}$-in. by 6-in. by 12-in. plastic scintillation counters and one $\frac{1}{4}$-in. by 1.5-in. by 10-in. defining counter, all viewed by RCA 6810 A photomultiplier tubes. A $\frac{1}{4}$-in. by 6-in. by 11-in. scintillation counter was placed behind the liquid-hydrogen target to detect those particles that did not stop in the target. A $\pi_1\pi_2\pi_3\bar{\pi}$ signal was required to obtain a π count. The gamma counters consisted of 19 alternate layers of plastic scintillator (10 layers) and lead (9 layers), each of dimensions $\frac{1}{8}$ in. by 11 in. by 23 in. Alternate layers of scintillator were viewed on the $\frac{1}{8}$-in. by 11-in. surface by one RCA 7046 phototube through a polished aluminum (Alzak) light pipe. Only one end of each scintillator was exposed to a phototube so that, if necessary, a coincidence could be required between the signals from alternate layers to eliminate heavily ionizing particles. During the experiment this proved unnecessary and signals from the two ends were added together. Two of these counters were placed above the liquid-hydrogen target and separated from it by 11 in. The gamma counters subtended approximately 12% of the total solid angle around the target; the calculated efficiency of these counters was 80%—based upon the thickness of the lead used and the pulse-height spectrum observed.

The neutron counter consisted of a 1-in. by 15.5-in. disk of terphenyl-plastic scintillator viewed by 7 RCA 7046 photomultiplier tubes through a 6-in.-thick Lucite light pipe optically sealed to the phototube face with Dow Corning silicone grease. Between the light pipe and the tubes was placed a 1-in. thick lead plate with a 3.5-in. hole centered over each tube. Surrounding the scintillator and phototubes on the sides and bottom was a 1-in.-thick lead shield. Surrounding the sides and top of the phototube volume was a $\frac{1}{8}$-in.-thick μ-metal magnetic shield. The counter and shields were enclosed in an iron container with an attached refrigerator, the latter for the purpose of reducing dark current from the phototubes. A 0.020-in.-thick μ-metal dome formed the top of the container. The thick light pipe and lead plate served to shield the scintillator from radioactivity (primarily from Ra in equilibrium with its decay products) emanating from the phototube glass. The outer lead shield reduced by a factor of nine that portion of the external background not associated with beam intensity. A drawing of the neutron counter is shown in Fig. 3.

All components inside the lead shield and the shield itself were tested for background radioactivity in a low-background room. The lead chosen was from the St. Joseph lead mine, and was found to be well below the average in radioactivity of lead from other sources.

The voltages for each of the seven phototubes were set to minimize the cathode transit-time spread over a 3.5-in.-diam circular area centered on the tube face. Outside this region the collection efficiency is very low for this tube, and masking off the outer region has the primary effect of eliminating infrequent pulses with large transit times. The transit-time spread over the central region was minimized in the following manner: light pulses from a Lawrence Radiation Laboratory pulsed mercury-discharge lamp[8] were attenuated until only single photoelectrons were detected. Under this condition the voltages in the cathode end of the tube were varied until the transit-time differences were minimized. The rms transit-time spread averaged over all seven tubes used was reduced by this technique to 3.4 nsec for single photoelectrons arriving at the first dynode of the tube. The following fractions of the anode-cathode voltage were found to satisfy the above conditions for a typical tube: cathode to grid 1, 3.9%; grid 1 to grid 2, 26%; grid 2 to dynode 1, 1.3%; between dynodes, 4.9%. In the assembled counter, the rms time spread was 2.9 nsec, averaged over the 400-keV neutron

[8] For a description of equipment see the Lawrence Radiation Laboratory Counting Handbook, UCRL-3307 Rev., 1959 (unpublished).

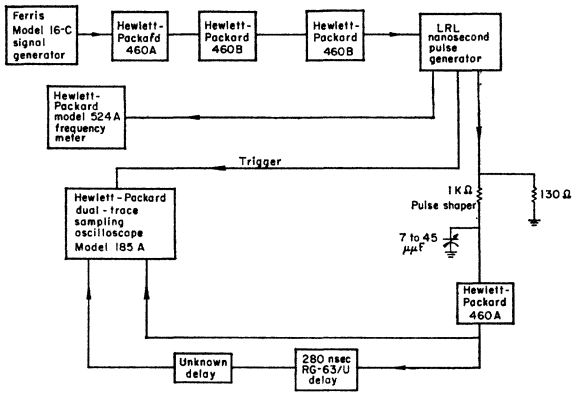

FIG. 4. Circuit diagram for delay measurement.

pulse-height distribution. The coincidence-detection efficiency for the slow-neutron pulse-height range was 66%, and was 96% for the fast-neutron pulse height.

The seven phototube signals from the neutron counter were summed in a distributed adder which gave a linear sum of the seven input signals, with a gain of unity for a single input. The input signals were lined up with short-delay cables in order to minimize the time spread in the output signal. The amplified output of this adder was displayed on the oscilloscope. Alternate tubes in the outer ring were added in two threefold adders similar to the sevenfold adder, and any combination of alternate tubes was able to satisfy the trigger requirement. The rate of accidental coincidences due to dark current in the six outer tubes was 800 counts/min with the refrigerator operating—a value lower by a factor of 10 than the real background. The refrigerator reduced the singles rate from individual tubes by a factor of six, on the average, from the room-temperature rate.

C. Auxiliary Equipment

The delay lines used to delay the γ-counter signal consisted of two sections: (a) the trigger delay, labeled "$\pi\gamma$ delay" on the circuit diagram (Fig. 2), which utilized up to 3 μsec of $1\frac{5}{8}$-in. Prodelin coaxial cable,[9] (b) the oscilloscope γ-signal cable, which consisted of approximately the same length of 2-in. Styrofoam-dielectric cable manufactured at the Lawrence Radiation Laboratory. Two microseconds of delay cable attenuated the γ-signal pulse height approx 20%. The γ-signal cable was enclosed in a temperature-controlled room which maintained the temperature constant within ± 1°C, or the total time-delay constant within ± 0.04 nsec.

The delay of the cable used was measured with an artificial pulse designed to simulate the phototube-output pulse shape. The cable-measuring circuit is shown in Fig. 4. The output of the driven pulser was split and one pulse was displayed directly on a Hewlett-Packard dual-trace sampling oscilloscope. The other pulse was displayed on the remaining trace after traveling through the unknown delay. The oscillator frequency was varied until the time between half heights of successive pulses was equal to the unknown delay time. In this condition the half height of successive pulses coincide on the oscilloscope face. The change in the artificial pulse shape due to frequency-dependent attenuation in the delay line is equal to the change in the actual phototube pulse if the two pulses are identical —the degree to which this was achieved is discussed in the section on errors. The cable delay was given by the reciprocal of the above frequency. Each cable was measured more than one time; the rms measurement error determined in this way was 0.05 nsec.

The changes in flight-path length were measured with a calibrated metal tape used at constant tension and temperature. The tape correction factor at all positions used was found to be 0.999966, as determined from a standard tape obtained at the Lawrence Radiation Laboratory, Livermore, California.

At the 17-ft depth the signal-to-background ratio of the data at a fixed beam intensity was proportional to the fractional spillout time of the meson beam. In order to maximize this ratio, the recently installed cyclotron auxiliary dee was utilized—with which the effective duty cycle was increased from 3% to more than 50%. At depths greater than 30 ft, the background level in the neutron counter was essentially independent of the meson-beam intensity.

The 517 A oscilloscope was time-calibrated by photographing the amplified output of a sine-wave signal generator operating at 100.17 Mc and at 150.04 Mc. The sweep speed measured in this way was indeterminate to approx 0.3%, over the portion of the scope face used during the data taking.

The neutron-counter magnetic shielding reduced the field at the position of the photomultiplier tubes to less than 100 mG transverse to the axes of the tubes, and to less than 150 mG along the axes of the tubes. The magnetic field varied from these upper limits to approximately zero, depending upon the position of the neutron counter relative to the cyclotron. However, the operating characteristics of the photomultiplier tubes showed no detectable changes attributable to the magnetic-field variation. The quantities measured accurately were transit-time spread and time delay. In addition, the pulse height was roughly determined and found to be constant.

IV. RESOLUTIONS AND COUNTING RATES

The electronic resolution of the neutron counter was measured with the aid of a pulsed hydrogen discharge lamp which was installed in the scintillator and pulsed at a rate of 300 times a second, with a pulse width of 2 nsec. The light intensity was adjusted to correspond

[9] Manufactured by Prodelin, Inc., Kearny, New Jersey. This cable has an impedance of 125Ω and an attenuation at 100 Mc of 3 dB per 1000 ft.

to the measured slow-neutron pulse-height spectrum and then the output of the sevenfold adder was photographed along with a trigger signal taken from the pulser. The oscilloscope trace was triggered by a coincidence between any two alternate phototubes in the neutron counter. This requirement imposed the same restrictions on time jitter as those found during the data-taking runs. The measured time differences between pulser trigger signal and sevenfold output signal yield the intrinsic electronic resolution of the neutron counter. The rms width was measured at 17, 47, and 67 ft in order to determine any change in this quantity with position. The rms deviation about the mean remained constant at 2.90±0.13 nsec at these depths.

The resolution of the γ-counter plus neutron-counter system was measured by the simultaneous detection of the two γ rays from neutral pion delay. The electronic resolution of the neutron counter for γ-ray pulse height was measured as before, by using the light pulser adjusted to yield the proper pulse-height range. The rms width for the neutron counter alone was 1.3±0.08 nsec for this pulse-height range. The total $\pi^0-\gamma$ resolution width was 2.8±0.12 nsec, from which we find the intrinsic rms width of the γ counters alone to be 2.5 nsec for the pulse-height range of the slow-neutron runs.

The rms spread in the flight time of slow neutrons due to finite target height was calculated on the assumption of a pion beam, uniform in intensity in the vertical direction, striking the 1-in.-high liquid-hydrogen target. The value obtained was 0.88 nsec. The same quantity for the 1-in.-thick plastic scintillator of the neutron counter was 0.82 nsec. By assuming Gaussian distributions, we find the total intrinsic resolution of the system for counting slow neutrons plus π^0-decay γ's to be

$$\sigma_T=(\sigma_{\gamma T}^2-\sigma_{n\gamma}^2+\sigma_{nn}^2+\sigma^2_{\text{target}}+\sigma^2_{\text{scintillator}}{}^2)^{1/2}$$

or

$$\sigma_T=(2.80^2-1.30^2+2.90^2+0.88^2+0.82^2)^{1/2}$$
$$=4.00\pm0.23 \text{ nsec},$$

where $\sigma_{\gamma T}\equiv$rms spread of the total system for counting π^0-decay γ, $\sigma_{n\gamma}\equiv$rms spread of the neutron counter for counting π^0-decay γ, $\sigma_{nn}\equiv$rms spread of the neutron counter for counting slow neutrons, and where we have used $\sigma_\gamma=(\sigma_{\gamma T}^2-\sigma_{n\gamma}^2)^{1/2}\equiv$rms spread of the γ counters for counting π^0-decay γ's. A numerical fold of the distributions from which $\sigma_{\gamma T}$ and σ_{nn} were obtained yields the result $\sigma_T=4.13\pm0.23$ nsec (shown in Fig. 5).

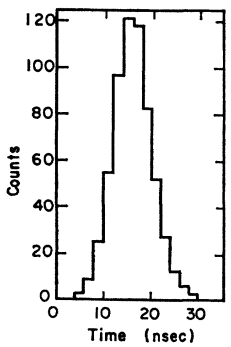

FIG. 5. Total-system resolution for detection of slow neutrons.

A direct measurement of σ_T was made by the following technique: The total resolution of the system was measured for the simultaneous detection of the two π^0-decay γ's with the normal pulse-height range accepted from the γ counters. For the neutron counter, only those signals were accepted that yielded the slow-neutron pulse-height spectrum. The value obtained was $\sigma_T=4.71\pm0.43$ nsec, which includes the artificial addition of the two terms σ_{target} and $\sigma_{\text{scintillator}}$. The best estimate of σ_T is taken to be 4.24±0.41 nsec.

The beam intensity was measured with a 1- by 10-in. scintillation counter placed at the position of the liquid-hydrogen-target center and in coincidence with $\pi 1$ and $\pi 2$. With 22 g/cm^2 of carbon placed in front of the small counter, data were obtained with the cyclotron running at reduced beam and with short target spill-out time. The average counting rate was 2.2×10^7 particles/min (extrapolated to full beam intensity). With the hydrogen target filled and in position, the coincidence rate between the π counters and the γ counters was measured as a function of beam-degrader thickness. The full width at half maximum of the resulting curve corresponded to an energy spread of 11 MeV before degradation, with the mean at 113 MeV. At full beam intensity and with the long duty cycle, 4×10^5 pions/min were stopped in liquid hydrogen.

The measured detection efficiency for those 400-keV neutrons that reached the neutron counter was 40%, which indicates that approximately 66% of the knock-on protons yielded a detectable light pulse. The measured detection efficiency for the 8.8-MeV neutrons was 22%, which corresponds to a light-pulse counting efficiency of 96% for the hydrogen and carbon nuclei struck by the higher-energy neutrons. The slow-neutron detection rate at 17 ft and at full beam intensity was 4.5 neutrons/min.

V. DATA AND ANALYSIS

Figures 6 through 11 show the time distributions obtained for 400-keV and 8.8-MeV neutrons. The abscissa represents the time difference in nsec between half-heights of the neutron-counter signal and the γ-counter signal, as observed on the oscilloscope face.

A determination of the neutron velocity from the mean time difference at each depth will be affected by changes in shape of the time distribution with depth. The effect of any *fixed* asymmetry in the intrinsic resolution of the equipment is to shift all distributions measured by this equipment by precisely the same amount.[10] This holds true exactly only if the distribution is measurable over the complete time range involved.

[10] K. M. Crowe, Ph.D. thesis, University of California Report UCRL-2050, 1952 (unpublished).

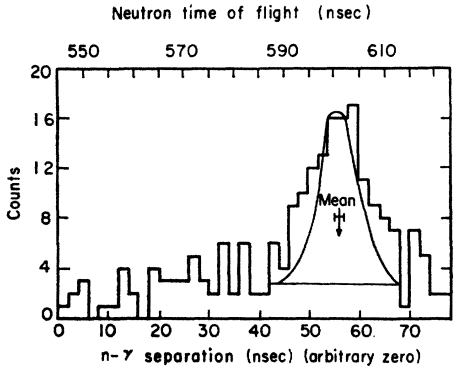

FIG. 6. Slow-neutron time distribution at 17 ft, Run I. Neutron PH $\leqslant$ 0.8 max; γ PH $\geqslant$ 0.40 max. The smooth curve represents the measured resolution function.

In the case of the 400-keV neutron, the rms deviation about the mean at 17 ft was found to be significantly larger than the σ_T given in Sec. IV. *The assumption is made* in analyzing the data that this added deviation is due to effects that yield a symmetrical velocity spread about the mean velocity. It is, therefore, assumed that all asymmetries arise from the shape of the intrinsic resolution of the equipment; that is, the distribution from which σ_T was obtained. The exception to the above symmetry that was considered and corrected for is that due to scattering of the neutrons in the target and in the atmosphere between target and counter.

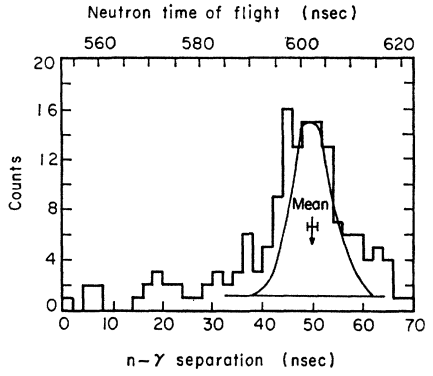

FIG. 7. Slow-neutron time distribution at 17 ft, Run II. Neutron PH $\leqslant$ 0.8 max; γ PH $\geqslant$ 0.40 max. The beam level for this run was approximately one-half that of Run I.

The resolution width of the oscilloscope-trigger coincidence circuit was set too narrow to cover the unexpectedly large spread in the slow-neutron velocity, and therefore the complete time distribution was not measured at 47 and 67 ft. At 47 ft only the high-velocity side was recorded on film to the full extent of the distribution. The low-velocity side was recorded only one-third of the distance from the peak to the limit of the spread. At 67 ft the peak was centered within the data taken, but neither wing was fully recorded.

The evidence that the slow-neutron time spread increased with depth comes from the following considerations:

(a) The expected time distribution as found from the light-pulser data at 17 ft may be compared to the measured neutron distribution at the same depth. The effect of a velocity spread is the smallest at this depth, but the full distribution was recorded. This comparison is made in Sec. VIII.

(b) This same comparison may be made by using the data from the detection of the γ rays from π^0 decay instead of the light-pulser data. As discussed in Sec. IV, only the low-pulse-height signal is accepted from the neutron counter in this comparison.

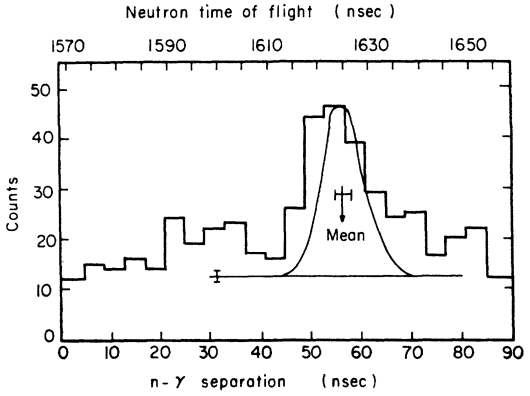

FIG. 8. Slow-neutron time distribution at 47 ft. Neutron PH $\leqslant$ 0.8 max; γ PH $\geqslant$ 0.32 max. The indicated background was determined from the expected neutron detection rate.

(c) A comparison of the expected *rate* of detection of slow neutrons at 47 ft (as calculated from the measured rate at 17 ft) may be made with the observed rate. Only one-third of the expected rate was found within a peak as narrow as that found at 17 ft.

(d) The expected background rate at 47 ft may be determined from the target-empty data. These data yielded an accurate determination of the background time distribution (see Fig. 12) and pulse height, but the background *rate* was too sensitive to the poorly known beam intensity for a useful result. The result agreed

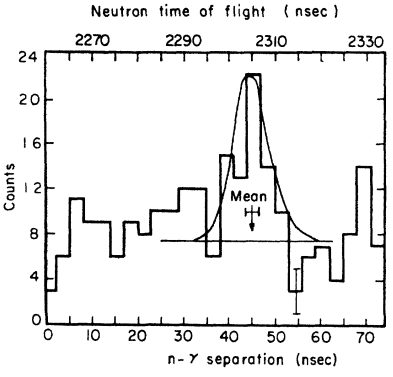

FIG. 9. Slow-neutron time distribution at 67 ft. Neutron PH $\leqslant$ 0.8 max; γ PH $\geqslant$ 0.32 max. The reduction in minimum γ PH compensates for the pulse-height attenuation in the delay cable.

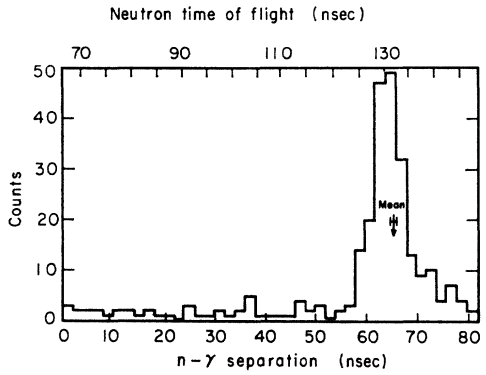

FIG. 10. Fast-neutron time distribution at 17 ft. Neutron PH $\geqslant$ 0.92 max; γ PH $\geqslant$ 0.50 max.

with the rate found in (c) above, but with a much larger uncertainty.

A calculation was made of the effect of the observed asymmetric resolution function upon the mean value of the velocity distribution. Since only part of the data was recorded at the lower depths, there is a shift in the observed mean compared with the 17-ft data, where the complete distribution is available. This calculation consisted in folding the measured intrinsic resolution function into a symmetric triangular velocity function. The mean was then calculated over the total distribution and also over the experimentally available portions. This permits a correction to be made to the data at the lower depths relative to the 17-ft data.

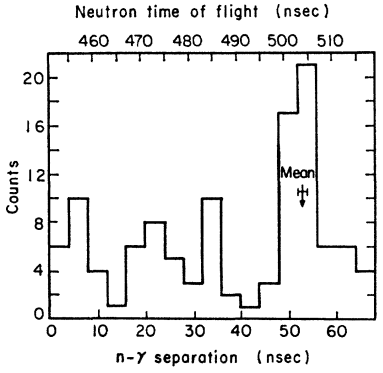

FIG. 11. Fast-neutron time distribution at 67 ft. Neutron PH $\geqslant$ 0.92 max; γ PH $\geqslant$ 0.46 max.

The following technique is used to determine the mean at all depths. From the target-empty data it is known that the detection efficiency is constant within a 70-nsec time region. A fixed point is selected within the constant-efficiency region and to one side of the visible peak in the data. This fixed point remains one extreme of the region over which the mean is taken. The mean is then computed over an arbitrary portion of the constant-efficiency region which encompasses the peak. A new region is then selected that is symmetrical about the computed mean and with the fixed point as one extreme. By repeating this process, a mean value is asymptotically arrived at which is centered within the region sampled. A uniform background was subtracted in all cases. The results of this analysis are shown in Table I.

Figure 13 shows the neutron-counter pulse-height distribution in the region of the 400-keV neutron peak at 17 ft. The flat distribution from 0.1 to 0.8 maximum is taken as the knock-on proton pulse-height distribution. The cutoff at 0.1 maximum is due to scanner bias against the small difficult-to-read pulses. A plot of the data with pulse height greater than 0.8 maximum gave no evidence of a peak in the time distribution and these data are assumed to be background. The average signal-to-background ratio up to 0.8 maximum is 3.8 in this time region.

VI. CORRECTIONS AND ERRORS

The largest calculated correction to the observed data comes from the scattering of neutrons between

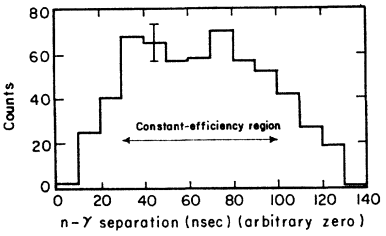

FIG. 12. Background time distribution with liquid-hydrogen target empty.

source and detector. It was assumed in making this correction that all interactions in the liquid hydrogen, iron, aluminum, and air are elastic-scattering events. At all depths the scattering from the hydrogen target structure, air, and hole walls results in a shift in mean flight time calculated to be less than 0.1 nsec. The calculated shift introduced by scattering from the liquid hydrogen is listed in Table I. Approximately 3% of the observed slow-neutron peak at 17 ft was due to neutrons scattered from hydrogen.

A calculation was made of the contribution to the spread in slow-neutron velocity due to pion-proton interactions in flight. At 90 deg to the incident pion beam, in the laboratory system, the velocity of slow neutrons from interactions in flight is lower than from interactions at rest. For a pion energy of 8 MeV, the neutron velocity is reduced 5%. For greater reductions than this, the neutrons will not be observed within the zero-pion-energy peak. The fraction of pions that inter-

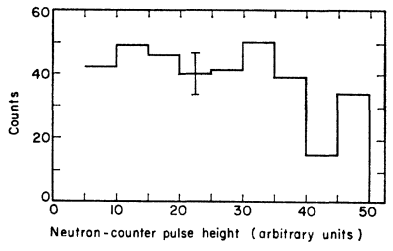

FIG. 13. Slow-neutron pulse-height distribution—neutron counter.

TABLE I. Summary of data and calculations.[a]

	Units	400-keV neutron 17 ft Run I	400-keV neutron 17 ft Run II	400-keV neutron 47 ft	400-keV neutron 67 ft	8.8-MeV neutron 17 ft	8.8-MeV neutron 67 ft	π^0 decay gamma 17 ft	π^0 decay gamma 47 ft	π^0 decay gamma 67 ft	Reference section
Measured data											
γ delay (single arbitrary zero)	nsec	1054.77	1079.75	2055.27	2759.86	579.00	966.36	478.80	503.89	515.47	III
Tape[b]	ft	14.676	14.680	44.682	64.668	14.672	64.671	14.669	44.682	64.673	III
γ-n separation[c]	mm	+2.72	+40.23	−32.47	+10.85	+0.85	+25.66	+27.79	+18.83	+4.82	V
Number of events		100	110	125	33	200	27	249	101	197	
Corrections											
Tape	ft	−0.0005	−0.0005	−0.0015	−0.0022	−0.0005	−0.0022	−0.0005	−0.0015	−0.0022	III
Scattering	nsec	−0.30	−0.26	−0.06	0	−0.10	−0.02	0	0	0	VI
Resolution asymmetry	nsec	0	0	−0.03	−0.14	0	0	0	0	0	V
Shift with depth	nsec	0	0	+0.19	+0.21	0	+0.21	...	...	...	VI
Delay	nsec	0	0	+0.32	+0.32	+0.26	+0.23	+0.13	+0.13	+0.17	VI
Detection-efficiency change	nsec	+0.23	+0.14	0	0	+1.04	+0.74	+0.60	+0.33	+0.53	VI
Errors (all ±)											
Delay reading	nsec	0.05	0.05	0.08	0.08	0.05	0.05	0.05	0.05	0.05	III
Tape reading	nsec	0.03	0.03	0.03	0.03	0	0	0	0	0	VI
γ-n separation	nsec	0.87	0.87	1.45	1.50	0.28	0.90	0.21	0.32	0.25	VI
Scattering	nsec	0.10	0.10	0.05	0.05	0.03	0	0	0	0	VI
Resolution asymmetry	nsec	0	0	0	0.05	0	0	0	0	0	V
Shift with depth	nsec	0	0	0.39	0.34	0	0.34	...	...	...	VI
Scope calibration[d]	nsec	0	0.07	0.06	0.02	0	0.04	0.04	0.04	0.01	III
Delay temp. change	nsec	0.01	0.01	0.03	0.04	0	0	0	0	0	VI
Detection-efficiency change	nsec	0	0	0.06	0.06	0	0.09	0	0.10	0.02	VI
γ PH bias level	nsec	0	0	0.03	0.03	0	0.15	0	0	0	VI

[a] All errors and corrections $\leqslant 0.01$ nsec are listed as "0."
[b] Add 2.90 ft to tape reading to obtain actual separation between liquid-hydrogen center and scintillator center.
[c] The separation is given in mm as read directly from the film-scanning machine (1 mm ≈0.6 nsec).
[d] The error listed refers only to the error on the γ-n *separation* due to the uncertainty in sweep speed.

acted with $0<T_\pi<8$ MeV was calculated to be less than 0.3% relative to the total number of interactions. Interactions in flight, therefore, have a negligible effect upon both the mean and the dispersion about the mean for the data obtained.

The correction labeled "Shift with depth" in Table I was obtained from the time of flight of the $\pi^0\gamma$ rays. The shift, which was 0.2 ± 0.4 nsec, is assumed to be independent of pulse height for values ranging from γ pulse height to slow-neutron pulse height. The magnetic field at the position of the neutron counter phototubes was less than 100 mG transverse to the axes of the tubes, a value which results in less than 1% reduction in pulse height, and should have a negligible effect on the transit time of the tubes.

The correction to the delay measurement was made to compensate for the improper pulse shape of the original pulse used to measure the delay cables. Each delay length was redetermined for various measuring-pulse rise times, and the difference in delay corresponding to the difference in rise time between the real phototube pulses and the original measuring pulse is listed.

The correction listed as "Detection-efficiency change" allows for the variation in detection efficiency as a function of n-γ separation as determined from the target-empty background runs. The correction was determined by dividing the observed particle-detection rate by the relative efficiency, and recomputing the mean flight time.

The error listed as "Tape reading" in Table I represents the flight time over one-fifth of a minor division on the calibrated tape.

The estimate of the "γ-n separation" error was arrived at by fitting a postulated distribution to the observed data at each depth. The χ^2 probability was calculated for various positions of the postulated peak relative to the observed peak—the error listed represents one-half of the minimum time needed to span 68% of the resulting probability distribution. The postulated distribution at 17 and 67 ft consisted of a flat background plus the measured resolution function normalized to minimize χ^2. The fit to the 67-ft slow-neutron data using the postulated peak plus background is greater than fifty times more likely than a flat distribution at the average number of counts. At 47 ft, the wider peak was fitted with a Gaussian distribution plus flat background. The above method allows a check to be made on the mean n-γ time difference arrived at as in Sec. V. In all cases the two methods agreed within one-third of the final error.

The error labeled "Delay temperature change" represents the change in delay time caused by a ±1°C temperature variation in the temperature-controlled delay house.

The "γ pulse-height bias level" error arises from the inability to determine precisely the γ pulse-height attenuation vs delay length.

VII. CALCULATION OF PION MASSES

A. Mass Difference, $m_{\pi^-}-m_{\pi^0}$

If the binding energy between negative pions and protons is taken to be zero, then the pion mass difference is given by

$$\Delta\equiv m_{\pi^-}-m_{\pi^0}=m_{\pi^-}-[(m_{\pi^-}+m_p)^2+m_n^2 -2\gamma_n{}^s m_n(m_{\pi^-}+m_p)]^{1/2}\ \mathrm{MeV}/c^2,$$

where $\gamma_n^s=[1-(\beta_n^s)^2]^{-1/2}$, β_n^s is the velocity of the slow neutron in units of the velocity of light. From the work of Day *et al.*[11] and Russell and Shaw[12] on the capture time of pions in hydrogen it is found that negative pions undergo the strong interaction with protons from n levels greater than 2. Therefore, the average binding energy is probably less than 360 eV. Since this number is small compared with the errors involved in the mass determination, it is set equal to zero in the calculation above. Another small correction, on the order of 50 eV (due to the finite π^--p center-of-mass velocity at the time of the interaction, as discussed in Sec. VIII), is also neglected.

The error on the mass difference is given by

$$S_\Delta=\frac{1}{m_{\pi^0}}\{(m_{\pi^-}-\delta)^2S_\delta^2+(\Delta-\delta)^2S_{m_{\pi^-}}^2+[m_n(m_{\pi^-}+m_p)(\beta_n^s)^2]^2(S_d^2/d^2+S_t^2/t^2)\}^{1/2}\ \mathrm{MeV}/c^2,$$

where $\delta=m_n-m_p$, d is the slow-neutron flight distance, and t is the slow-neutron flight time. In this formula the approximation $\gamma_n^s=1$ is used. Therefore,

$$S_\Delta=[(1.024)^2S_\delta^2+(0.0237)^2S_{m_{\pi^-}}^2+(6.52)^2(S_d^2/d^2+S_t^2/t^2)]^{1/2}\ \mathrm{MeV}/c^2.$$

From Table I, the following information is obtained (see Appendix):

From 17 ft to 47 ft: $v_n^s=0.029384$ ft/nsec,
$\Delta=4.6030$ MeV/c^2,
$S_\Delta=0.0102$ MeV/c^2.

From 17 ft to 67 ft: $v_n^s=0.029400$ ft/nsec,
$\Delta=4.6067$ MeV/c^2,
$S_\Delta=0.0065$ MeV/c^2.

The weighted average of Δ is

$$\Delta=4.6056\pm0.0055\ \mathrm{MeV}/c^2$$
or 9.013 ± 0.011 electron masses.

B. Negative-Pion Mass

If we again neglect the π^--p binding energy, we have

$$m_{\pi^-}=\gamma_n^F m_n(1+\beta_n^F)-m_p\ \mathrm{MeV}/c^2,$$

where β_n^F is the velocity of the 8.8-MeV neutron in units of the velocity of light. The error (squared) on the pion mass is

$$S_{m_{\pi^-}}^2=[(\gamma_n^F)^3m_n(1+\beta_n^F)(\beta_n^F)^2+\gamma_n^F m_n\beta_n^F]^2\times[S_d^2/d^2+S_t^2/t^2]+[\gamma_n^F(1+\beta_n^F)]^2S_{m_n}^2+S_{m_p}^2\ (\mathrm{MeV}/c^2)^2,$$

or

$$S_{m_{\pi^-}}=[150^2(S_d^2/d^2+S_t^2/t^2)+1.14^2S_{m_n}^2+S_{m_p}^2]^{1/2}\ \mathrm{MeV}/c^2.$$

From Table I we find

$v_n^F=0.13432$ ft/nsec,
$m_{\pi^-}=139.69$ MeV/c^2 or 273.38 electron masses,
$S_{m_{\pi^-}}=0.41$ MeV/c^2 or 0.80 electron masses.

The values used in the above error calculations were

$S_\delta=0.4$ keV/c^2,[13]
$S_{m_{\pi^-}}=56$ keV/c^2,[6]
$S_d=0.001$ ft,
$S_{m_p}=10$ keV/c^2,[6]
$S_{m_n}=10$ keV/c^2.[6]

VIII. SLOW-NEUTRON VELOCITY SPREAD

The evidence concerning the existence of the unexpectedly large spread in the slow-neutron velocity is listed in Sec. V. The most probable rms time spread due to the measuring equipment is shown in Sec. IV to be $\sigma_T=4.2\pm0.4$ nsec. In order to obtain the best estimate of the slow-neutron velocity spread at the 17-ft position, the rms spread of the signal minus background was calculated by using only the "fast" half of the data and including the background region. As the time region over which σ is calculated increases from zero, σ increases throughout the region of the velocity peak and then assumes an approximately constant value when the background region is included. The average of this approximately constant value from runs I and II at the 17-ft position is $\sigma_{17}=6.2$ nsec. From this we find the residual rms deviation to be $\sigma_{R17}=4.5$ nsec, which corresponds to an rms velocity spread of 6.5×10^6 cm/sec. The corresponding quantities at 47 ft are $\sigma_{R47}=17.6$ nsec and 9.5×10^6 cm/sec. Because of the possible large systematic errors involved in these determinations, the assignment of a reasonable error on purely statistical grounds is unreliable, so the final estimate of the velocity spread is taken to be $(8.0\pm1.5)\times10^6$ cm/sec.

The possible explanations for the observed residual deviation are listed below, along with their expected magnitudes.

(a) Variation in flight path due to finite target and scintillator size. This effect varies from approximately $\sigma=0.5$ nsec at 17 ft to $\sigma=0.2$ nsec at 47 ft, and, therefore, is of the wrong sign and too small to explain the observed effect.

(b) Slow-neutron scattering. At the 17-ft position the correction of the data for scattering reduces the rms deviation by 0.23 sec.

(c) Unknown π^--p binding energy. If it is assumed[10] that the pion is captured by the proton from an n level

[11] T. B. Day, G. A. Snow, and J. Sucher, Phys. Rev. Letters **3**, 61 (1959); and University of Maryland Physics Department Technical Report No. 159; T. B. Day, Report No. 175; G. A. Snow, Report No. 196 (unpublished reports).

[12] J. E. Russell and G. L. Shaw, Phys. Rev. Letters **4**, 369 (1950).

[13] R. O. Bondelid, J. W. Butler, C. A. Kennedy, and A. del Callar, Phys. Rev. **120**, 887 (1960).

greater than or equal to 3, then the maximum possible variation in binding energy is 360 eV. This corresponds to a maximum variation in flight time at 17 ft of 0.03 nsec.

(d) Neutral-pion mean life. The presently accepted value[14] of the π^0 mean life is $(1.9\pm0.5)\times10^{-16}$ sec. This value corresponds to an uncertainty in the time flight of slow neutrons over a 50-ft flight path of less than 0.01 nsec.

(e) π^--p thermal motion. The rms velocity to be expected for π^--p atoms in thermal equilibrium with liquid hydrogen at 20°K is 7×10^4 cm/sec, which corresponds to an rms time spread of 0.04 nsec at 17 ft and 0.1 nsec at 47 ft.

(f) Radiative deexcitation of the π^--p atom. The maximum velocity that the π^--p atom can attain from the recoil due to radiative deexcitation is 9×10^4 cm/sec, and is probably less than 1×10^4 cm/sec. This yields a negligible time spread at all depths.

(g) Collisional de-excitation of the π^--p atom. The remaining process believed to be capable of explaining the large observed velocity spread is that investigated by Day *et al.*[11] and Russell and Shaw.[12] They find that the experimentally observed π^- capture time[15] can be explained in terms of the slowing-down process described by Wightman[16] with the addition of Stark-effect reshuffling of the l levels for n values of 3 to 5. This latter process is very fast compared with radiative de-excitation, and brings about the capture of π^- mesons in S states of pricipal quantum numbers 3 to 5. In the calculations above, the authors assumed a velocity of the π^--p system of 10^5 to 10^6 cm/sec, as obtained from estimates of the collisional deexcitation energy. According to Day,[17] velocities of 10^7 cm/sec are compatible with the experimental results of π^- capture times and with the theoretical results of the slowing-down process.

The last effect [item (g)] is believed to be the only one capable of explaining the large observed velocity spread.

IX. SUMMARY

1. The $m_{\pi^-}-m_{\pi^0}$ is 4.6056 ± 0.0055 MeV/c^2, based upon the following assumptions:

(a) The spatial distribution of stopping pions in the liquid hydrogen did not change with time.

(b) The average time from initiation of events to their detection at a fixed distance did not vary with time. Such a variation could be brought about by changing photomultiplier-tube voltages. During the runs at 67 ft, one tube in the neutron counter was turned off. This could yield a shift of up to 0.2 nsec, which corresponds to one-fourth of a standard deviation shift in flight time.

(c) The observed spread in slow-neutron velocities was symmetrical about the calculated mean. If the observed spread in velocity is due to center-of-mass motion of the π^--p system, there is a corresponding negligible shift in the flight time from the at-rest value.

(d) The frequency-meter crystal used in the delay-length determinations did not vary during these determinations more than the total long-term variation observed for this crystal. The observed variation corresponded to less than 0.01 nsec.

(e) The strong interaction between pion and proton occurred from bound atomic n levels greater than 2.

2. The m_{π^-} is 139.69 ± 0.41 MeV/c^2, based upon assumptions (a), (b), (d), and (e).

3. The rms deviation about the mean slow-neutron velocity corresponds to a rms velocity of the π^--p system of $(8.0\pm1.5)\times10^6$ cm/sec, with a distribution as shown in Fig. 8. This distribution includes the resolution function of the measuring equipment and the spatial distribution of the center-of-mass velocity.

ACKNOWLEDGMENTS

I would like to thank Professor K. M. Crowe for the valuable guidance and assistance offered by him throughout this experiment. A great deal of the original work with the equipment used in this experiment was done by Professor R. P. Haddock, and his interest until completion is appreciated. In addition, I would like to thank Professor Alexander Abashian, Dr. James Ryan, and John L. Whitsell for valuable help during the running of the experiment, and Roger Brown for the delay measurements. James T. Vale and Lloyd B. Hauser and the cyclotron crew under their supervision provided a reliable cyclotron beam throughout the experiment.

APPENDIX

The velocity was calculated from the data of Table I in the following manner. Let

$$T_l=[\gamma\text{ delay}-|\text{scattering}|-|\text{resolution asymmetry}|+|\text{shift with depth}|+|\text{delay correction}|+|\text{detection-efficiency change}|]\text{ nsec}-[\gamma\text{-}n\text{ separation}]\text{ mm},$$

where T_l is the time of flight to within an unknown additive constant (which remains fixed for a fixed velocity). The mm units of the γ-n separation are retained because of the nonlinear oscilloscope sweep speed and the subtraction which must be made from the data at a different position.

If we let $T_l\equiv A_l(\text{nsec})-B_l(\text{mm})$, then the absolute flight time from l to l' is

$$\Delta T=(A_{l'}-A_l)-(B_{l'}-B_l)S_{x',x}\text{ nsec},$$

where $S_{x',x}$ is the number of nsec per mm from x' to x on the oscilloscope face.

[14] R. G. Glasser, N. Seeman, and B. Stiller, Phys. Rev. **123**, 1014 (1961).
[15] T. H. Fields, G. B. Yodh, M. Derrick, and J. G. Fetkovich, Phys. Rev. Letters **5**, 69 (1960).
[16] A. S. Wightman, Phys. Rev. **77**, 521 (1950); and Ph.D. thesis, Princeton University, 1949 (unpublished).
[17] T. B. Day (private communication).